ORCA – Online Research @ Cardiff

This is an Open Access document downloaded from ORCA, Cardiff University's institutional repository:https://orca.cardiff.ac.uk/id/eprint/141778/

This is the author's version of a work that was submitted to / accepted for publication.

Citation for final published version:

Guillena, Estefania, Li, Wantao, Montoro, Gabriel, Quaglia, Roberto and Gilabert, Pere L. 2022. Reconfigurable DPD based on ANNs for wideband load modulated balanced amplifiers under dynamic operation from 1.8 to 2.4 GHz. IEEE Transactions on Microwave Theory and Techniques 70 (1) , pp. 453-465.

Publishers page: https://doi.org/10.1109/TMTT.2021.3091672

Please note:
Changes made as a result of publishing processes such as copy-editing, formatting and page numbers may not be reflected in this version. For the definitive version of this publication, please refer to the published source. You are advised to consult the publisher's version if you wish to cite this paper.

This version is being made available in accordance with publisher policies. See http://orca.cf.ac.uk/policies.html for usage policies. Copyright and moral rights for publications made available in ORCA are retained by the copyright holders.

Reconfigurable DPD Based on ANNs for Wideband Load Modulated Balanced Amplifiers Under Dynamic Operation From 1.8 to 2.4 GHz

Estefanía Guillena, *Student Member, IEEE,* Wantao Li, *Student Member, IEEE,* Gabriel Montoro, *Member, IEEE,* Roberto Quaglia, *Member, IEEE,* and Pere L. Gilabert, *Senior Member, IEEE*

***Abstract*—This paper proposes a methodology to ensure linear amplification of a load modulated balanced amplifier (LMBA) while keeping the power efficiency as high as possible over a frequency band ranging from 1.8 to 2.4 GHz and where the transmitted signals can present different bandwidth configurations. The proposed reconfigurable linearization methodology consists of, in a first step, tuning some free-parameters (with dependence on the signal bandwidth and frequency of operation) of the load modulated balanced amplifier (LMBA) to trade-off linearity and power efficiency. In a second step, two multi-purpose adaptive digital predistortion (DPD) linearizers are considered, properly combined with crest factor reduction (CFR) techniques, to meet the required linearity specifications. Either a DPD based on artificial neural networks or a DPD based on polynomials can be selected taking into account the compromise between computational complexity and linearization performance. Experimental results will validate the proposed methodology to guarantee the linearity levels (ACPR<-45 dBc and EVM<1%) with high power efficiency in an LMBA under dynamic transmission, where both the signal bandwidth (from 20 MHz and up to 200 MHz instantaneous bandwidth) and frequency of operation (in the range of 1.8 to 2.4 GHz) change.**

***Index Terms*—artificial neural network (ANN), digital predistortion (DPD), load-modulated balanced amplifiers (LMBA), power efficiency.**

I. INTRODUCTION

POWER-EFFICIENT amplification has been a hot research topic since the introduction of non-constant envelope digital modulations. Starting from W-CDMA in 3G, the peak-to-average power ratio (PAPR) of signals have kept increasing through the use of Orthogonal Frequency Division Multiplexing (OFDM) in 4G (LTE, LTE-Advanced), and now cyclic prefix OFDM in New Radio (NR) 5G. In addition, in order to satisfy the requirements for higher transmission rates, the signal bandwidths that the amplification architectures have to accommodate are always increasing (e.g., from a few MHz in 3G, to tenths of MHz in 4G, to hundreds of MHz in NR 5G). In addition, efficient amplification is required in several frequency bands in NR 5G with multiple numerology (i.e., subcarrier spacing) and channel bandwidths. This demands providing the baseband processing with some degree of reconfigurability to adapt to the changing transmission requirements.

When dealing with signals presenting high PAPR, the power amplifier (PA) needs to operate at large power back-off leading to a serious degradation of average efficiency. To avoid wasting excessive power resources, highly efficient amplification architectures based on dynamic load or dynamic supply modulation have been proposed in the literature. Some of the most popular solutions are envelope tracking PAs [1], Doherty PAs [2], [3], load modulated balanced amplifiers (LMBA) [4], [5] and LINC or outphasing PAs [6], [7]. In each case, these highly efficient topologies require the use of digital predistortion (DPD) linearization to guarantee the stringent linearity requirements of today's systems, especially with the increasing signal bandwidth.

All power amplifier architectures based on active load modulation, such as Doherty, LMBA and outphasing, rely on the non-linear interaction between multiple transistors to enhance the average efficiency in presence of modulated signals with large dynamic range. While these architectures can be designed with a single RF input to simplify their use in a transmitter, there are benefits in maintaining separate inputs controlled by different up-converter chains. Therefore, the additional degrees of freedom offered by the separate inputs can be used to optimize the performance on the same or larger bandwidth, or to improve other performance metrics such as linearity and average efficiency. In [8], for example, the authors propose the use of machine learning techniques to optimize the configuration parameters of a dual-input Doherty PA. Particularizing for dual-input LMBAs, the configuration of certain key free-parameters influencing the inherent linearity versus power efficiency trade-off is explored in [9], [10]. Among the different degrees of freedom that can be considered to optimize the LMBA performance, in [9] the authors proposed a method for predicting the optimum relative phase shift between the two input modulated signals to the LMBA that maximize linearity levels.

Some previous works published in literature addressing the linearization of LMBAs tested the PA with OFDM-based modulated signals but with moderate bandwidths (i.e., sev-

This work was supported in part by the Spanish Government (Ministerio de Ciencia, Innovación y Universidades) and FEDER (Fondo Europeo de Desarrollo Regional) under Grant TEC2017-83343-C4-2-R and in part by the Generalitat de Catalunya under Grant 2017 SGR 813. This paper is an expanded version from the International Workshop on Integrated Nonlinear Microwave and Millimetre-Wave Circuits (INMMiC), Cardiff, United Kingdom, July 2020.

E. Guillena, W. Li, G. Montoro and P. L. Gilabert are with the Department of Signal Theory and Communications, Universitat Politècnica de Catalunya (UPC) - Barcelona Tech, Barcelona, 08034, SPAIN, e-mail: estefania.guillena@estudiantat.upc.edu

R. Quaglia is with the Centre for High Frequency Engineering, Cardiff University, Queen's Buildings, The Parade, Cardiff CF24 3AA Wales, UK. e-mail: quagliar@cardiff.ac.uk

Manuscript received XX XX, 2021; revised XXX XX, 2021.

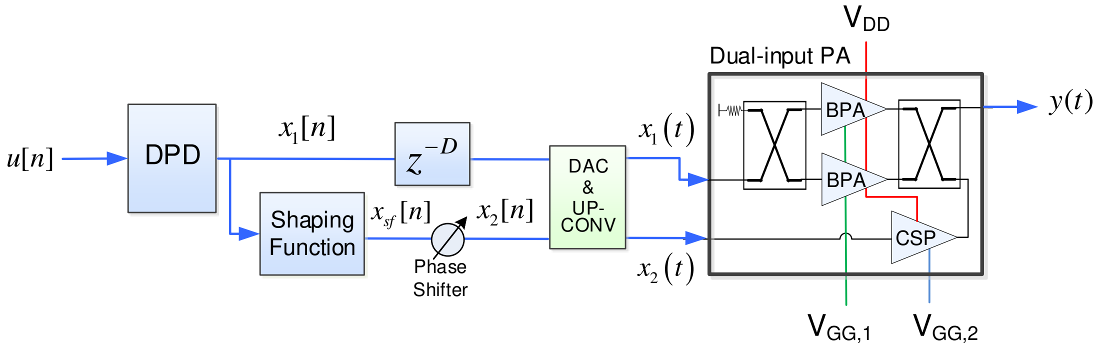

Fig. 1. Block diagram of the LMBA architecture with DPD linearization.

eral tenths of MHz), where the use of memory polynomial (MP), e.g., in [11], [12], or generalized memory polynomial (GMP), e.g., in [13], behavioral models was enough to meet the out-of-band linearity specifications. To the best authors knowledge, the linearization of LMBAs taking into account signal bandwidths of hundreds of MHz (thus, taking advantage of the broadband nature of LMBAs), up to now has been only addressed in [14] and [15]. On the one hand, in [14], the authors address the linearization of a supply-modulated LMBA when considering, among others, a NR-5G signal of 100 MHz instantaneous bandwidth. By considering a GMP-based DPD, the out-of-band linearization specifications cannot be met for the 100 MHz bandwidth signal. By using an ideal indirect learning control (sic), however, they show that the linearity specs could somehow be met. On the other hand, in [15], the authors presented the design and linearization of a LMBA that was tested with several OFDM-based signals taking into account bandwidths up to 200 MHz. With this last challenging bandwidth configuration of ten-carrier 200 MHz OFDM signal with 10 dB of PAPR, however, the reported adjacent channel leakage ratio (ACLR) after DPD linearization could not reach the threshold of -45 dBc using the magnitude-selective affine (MSA) function model for DPD. Moreover, none of the aforementioned papers addressing the linearization of LMBAs, provide information of the error vector magnitude (EVM) to quantify the in-band distortion, which may be of concern when operating PAs with broadband signals.

In this paper, a significant step forward is taken with respect to our previous work in [9], by proposing a methodology to ensure power efficient amplification from 1.8 GHz up to 2.4 GHz allowing reconfigurability to meet the linearity specifications in a dynamic environment, where the center frequency and bandwidth of the transmitted signal change. Consequently, in this dynamic environment, the adaptive DPD linearizer can be reconfigured by selecting different behavioral models according to the bandwidth of the signal. For example, when modeling strong nonlinearities with significant memory effects, the artificial neural network (ANN) DPD [16]–[18], can provide robust global estimation capabilities in contrast to the more local estimations provided by the polynomial-based DPD. For signal bandwidths of hundreds of MHz, we show in this paper that, given the difficulty of meeting the out-of-band linearity specifications when considering polynomial-based behavioral models, the use of ANNs for DPD linearization is justified. Therefore, unlike previously reported solutions, the ANN-based DPD proposed in this paper is capable to meet the ACPR specs (i.e., <-45 dBc) with EVM figures lower than 1% when considering 4 non-contiguous LTE-20 signals of 200 MHz total bandwidth.

Accordingly, the remainder of this paper is organized as follows. Section II presents a brief description of the LMBA used in this paper. Section III describes the proposed methodology to properly configure the free-parameters involved in the LMBA configuration to maximize linearity and power efficiency. Section IV describes the DPD linearization strategy followed, where both GMP and ANN-based DPDs are used. Details on the ANN configuration and the low-complexity adaptation strategy following a direct learning approach are also discussed. Section V describes the experimental test bench and shows experimental results including DPD linearization when considering a dynamic transmission environment (i.e., considering different center frequencies and signal bandwidths of the transmitted signal over a frequency band ranging from 1.8 GHz up to 2.4 GHz). Finally, the conclusion is given in section VI.

II. LOAD MODULATED BALANCED AMPLIFIER

In this paper, the LMBA presented in [5] is used as device under test (DUT). A simplified block diagram of the DUT and the DPD linearizer is shown in Fig. 1. There are two separate RF inputs; x_1 controls the balanced power amplifier (BPA) pair, based on two CGH40025F transistors from Wolfspeed, biased in class AB with $V_{\mathrm{GG},1}$ at -2.8 V corresponding to 80 mA of quiescent drain current; x_2 controls the control signal power (CSP) amplifier, also based on a CGH40025F, and biased in class C, with $V_{\mathrm{GG},2}$ left as a free parameter within the range of DC voltages -3.5 V to -5.5 V. The matching networks and the output hybrid couplers are based on soft-board microstrip networks, with SMD capacitors and resistors for the by-pass and stabilization networks. An off-the shelf hybrid is used on the input. The circuit is mounted on an aluminium fixture, and SMA coaxial launchers are used for the RF ports.

The CW measurements reported in [5] showed, over the 1.7–2.5 GHz frequency range, a maximum power larger than 63 W, and an 8 dB back-off efficiency exceeding 39%. Modulated signal measurements were also performed with 5 MHz and 20 MHz channel LTE signals, showing the linearizability of the LMBA under these conditions. Both sets of measurements were performed with a manual search for the optimum amplitude, phase and bias settings. In particular, the relative phase was maintained at a constant offset that led to a good compromise between output power and back-off efficiency, while the relative amplitude was following a square relation between the BPA and CSP inputs [5].

It is important to stress out that, when considering signals with bandwidths of several tenths or even hundreds of MHz with PAPRs exceeding 8 dB (e.g., typical PAPRs of carrier aggregated signals around 10 dB or higher), the average power efficiency shown by this particular LMBA decreases quite abruptly. However, the tuning and linearization methodology proposed in this paper is valid for addressing the inherent linearity versus power efficiency trade-off, independently on the specific power efficiency profile shown by the specific LMBA DUT.

The methodology proposed in this paper to cope with the LMBA linearity versus efficiency trade-off, when considering a dynamic scenario in which the transmitted signal configuration can change, in terms of bandwidth and frequency of operation in the range of 1.8 to 2.4 GHz, is depicted in the flow chart of Fig. 2. The first part of this flow chart corresponds to the tuning of the specific free-parameters of the LMBA (e.g., the phase shift or the amplitude relationship between the main and the auxiliary signal) that have an impact on its linearity and power efficiency. As it will be discussed in section III, the optimal value of these parameters depends on the signal bandwidth and frequency of operation. Once these parameters are properly tuned, in the second part of the flow chart (see Fig. 2), crest factor reduction (CFR) and adaptive DPD linearization techniques are applied to meet the required linearity specifications (i.e., ACPR < -45 dB) with the best possible power efficiency. Details on the architecture and adaptation process of the proposed DPD linearizers and the criteria to choose one over the other, will be discussed in section IV.

III. Configuration of the LMBA Free-Parameters

Some of the free-parameters of the dual-input LMBA that can be tuned to trade-off linearity and power efficiency are described in the following. Taking into account the notation in the block diagram of Fig. 1, the complex BPA signal is defined as $x_1[n] = x[n]$, where $x[n]$ is the signal at the output of the DPD. The complex CSP signal $x_2[n]$ is generated using a shaping function that controls the relative amplitude between the BPA and CSP inputs. More specifically, the CSP signal $x_2[n]$ is defined as

$$x_2[n] = x_{sf}[n]e^{i\Psi_{rel}} \tag{1}$$

where Ψ_{rel} is the relative phase in radians between the BPA and CSP signals; and where the signal after the shaping function $x_{sf}[n]$ is defined as

$$x_{sf}[n] = A_s[n]K_0e^{i\phi_x} \tag{2}$$

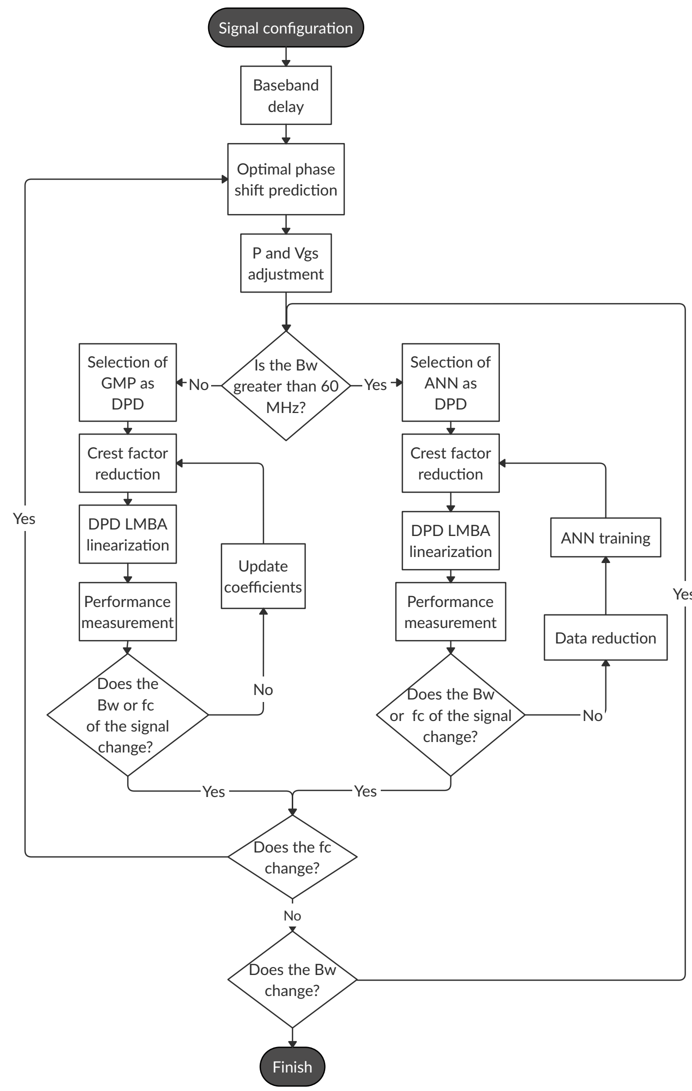

Fig. 2. Flow chart for the LMBA linearization and power efficiency enhancement.

where $K_0 = \frac{max\{|x[n]|\}}{max\{|A_s[n]|\}}$, $\phi_x = phase\{|x[n]|\}$ and the amplitude relationship between the two signals is given by the following expression, which is a simplified version of the shaping function used in [9], where $x_{min} = 0$ and thus,

$$A_s[n] = (|x[n]|^6)^{\frac{1}{p}} \tag{3}$$

with p being the degree of the root.

In order to determine the optimal value of some free-parameters such as the relative phase (Ψ_{rel}) or delay between the the BPA and CSP signals, or the degree of the root p; a 20 MHz bandwidth LTE signal (LTE-20) with a PAPR of 10.2 dB was used to evaluate the linearity and power efficiency when tuning these parameters. In addition, another free-parameter to be tuned is the gate voltage of the CSP amplifier, $V_{\mathrm{GG},2}$, that can be set to operate between a deep-class C condition that should favour efficiency, and a near-class B bias where linearity should improve.

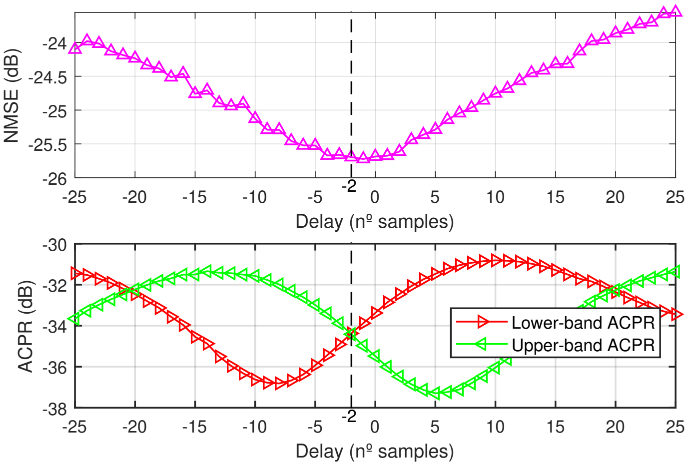

Fig. 3. NMSE, lower-band and upper-band ACPR for different delay samples between LMBA input signals.

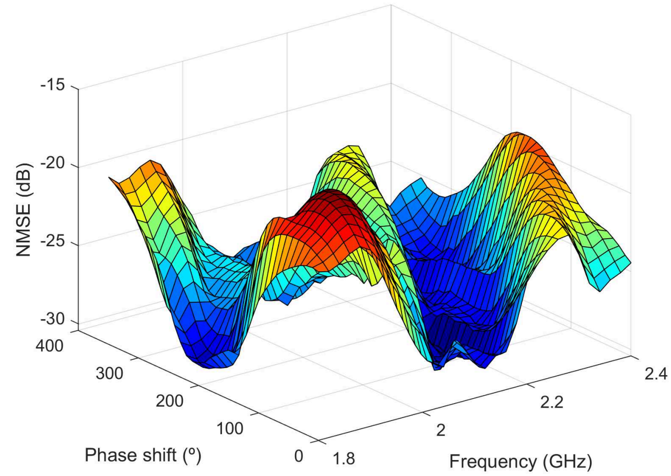

Fig. 4. NMSE value for different center frequencies and different phase shifts between the LMBA's input signals.

A. Selection of the Baseband Delay

In a first step towards the optimal tuning, the objective is to find a baseband time-delay between the LMBA inputs to balance the lower-band and upper-band ACPR of the LTE-20 test signal at the output of the LMBA. Fig. 3 shows the NMSE and ACPR of the amplified output for different delay samples between the LMBA inputs when considering the LTE-20 signal at 2 GHz center frequency, the optimum phase-shift in terms of linearity and p=3. As observed, the best NMSE values are for delays close to 0. However, without any delay, there is an ACPR difference of about 3 dB between the lower and upper bands. Therefore, for the sake of linearizability, a baseband delay of -2 samples is chosen to balance the ACPR in the lower and upper bands.

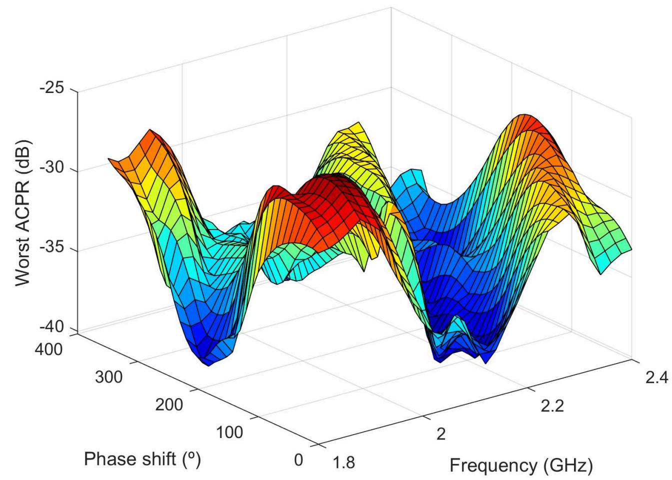

Fig. 5. Worst ACPR for different center frequencies and different phase shifts between the LMBA's input signals.

B. Estimation of the polynomial fitting to predict the optimal phase shift

As introduced in [9], the phase shift between the LMBA's main and auxiliary signals has a strong impact on its linearity. Consequently, selecting an optimal phase shift is of crucial importance, because with certain phase-shift configurations it is not possible to meet the linearity requirements even by applying DPD linearization. In addition, the optimal phase-shift depends on the specific frequency of operation.

Considering an LTE-20 test signal and fixing the degree of the root in (3) to $p = 3$, the effect on linearity of the phase shift between the LMBA's inputs for different center frequencies is shown in Fig. 4 and Fig. 5 in terms of NMSE and ACPR, respectively. However, as shown in Fig. 6, the power efficiency, despite having a strong dependence with the center frequency of operation (with its maximum value around 2 GHz), it is quite invariant with the phase shift between the LMBA inputs.

In terms of ACPR and NMSE, this optimal phase shift has a trend that can be predicted using a polynomial regression, as reported in [9]. In this paper, we have considered polynomial regressions of degrees 1, 3 and 5 and a piecewise regression of degree 1. Fig. 7 shows the measured upper and lower limit of the NMSE and ACPR over frequency when considering for each center frequency the worst and best phase shift, respectively. In addition, NMSE and ACPR values obtained with the predicted optimal phase-shifts using the different regression strategies are also shown. With all of them, the predicted phase-shift resulted in NMSE and ACPR values close to the lower bound for all the frequency range. However, the best prediction was obtained with a simple linear regression or the piecewise functions. From now on, these two regression approaches will be used to predict the optimal phase-shift in terms of linearity.

The polynomial regressions were extracted from data measurements of an LTE-20 signal. In order to validate that the optimal phase-shift predictions are valid when considering other signals with different bandwidths, Fig. 8 and Fig. 9 show the results for LTE signals with total bandwidths of 60 MHz and 200 MHz, respectively (further details on these test signals are given in section V). As observed, the NMSE and ACPR values obtained with the predicted optimal phase-shifts are very close to the optimal values (i.e., the lower bound) found

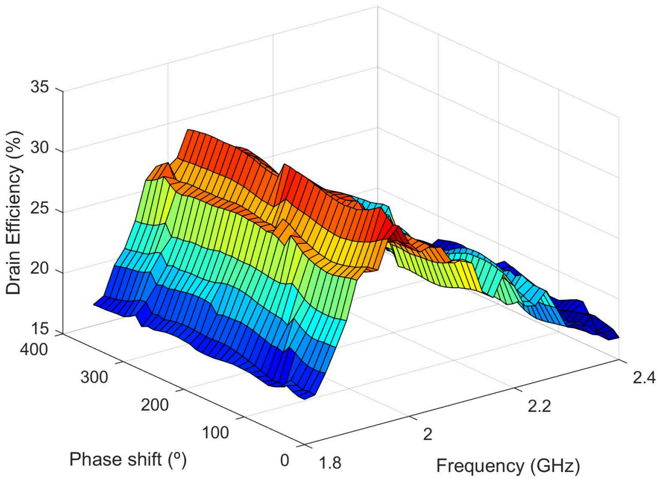

Fig. 6. Drain efficiency for different center frequencies and different phase shifts between the LMBA's input signals when considering an LTE-20 test signal with 10.2 dB of PAPR.

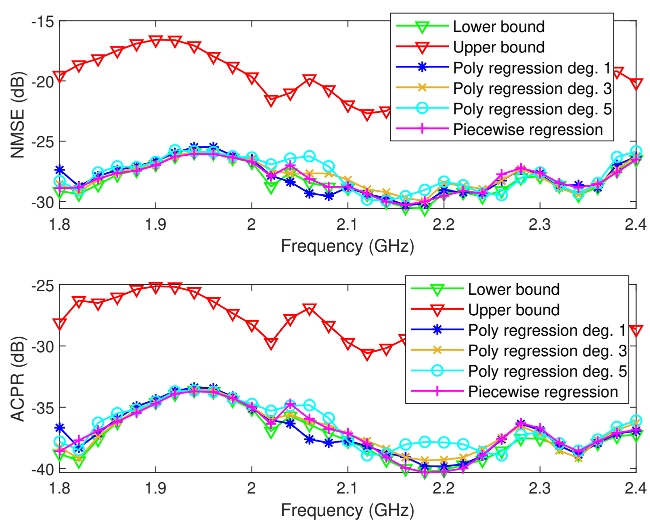

Fig. 7. NMSE and ACPR values obtained considering the predicted phase shifts taking into account different fitting approaches.

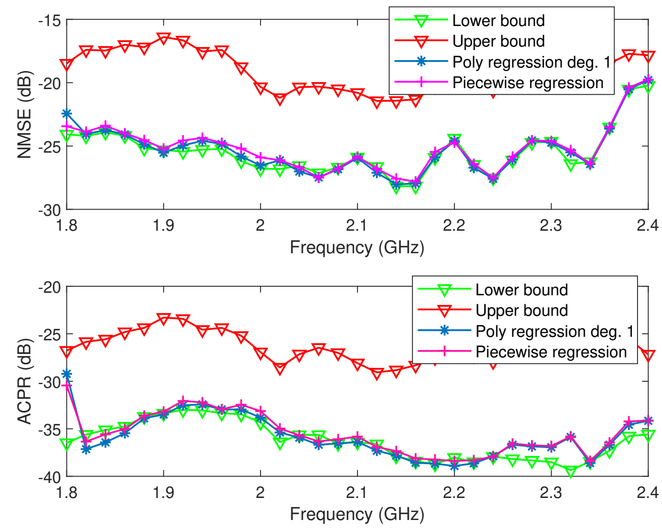

Fig. 8. NMSE and ACPR values for a NC 2×LTE-20 test signal of 60 MHz total bandwidth.

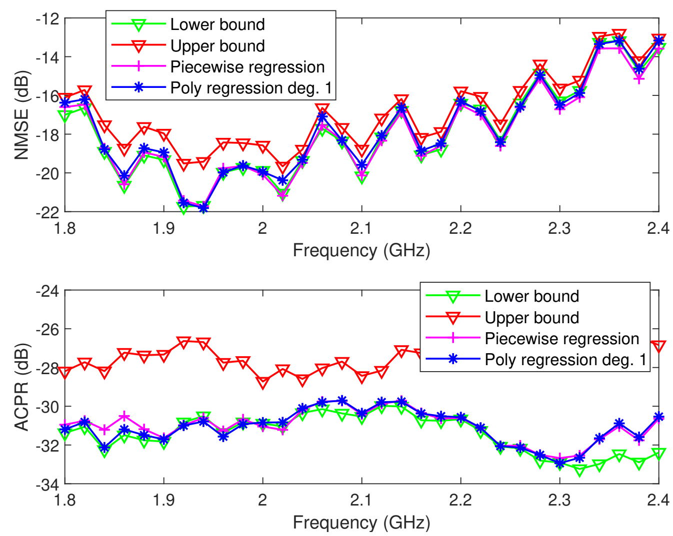

Fig. 9. NMSE and ACPR values for a NC 4×LTE-20 test signal of 200 MHz total bandwidth.

from measurements into the entire frequency range.

C. Selection of the optimal ranges of p and $V_{\mathrm{GG},2}$

The last step proposed to configure the LMBA consists of a fine tuning of the parameter p in (3) and the auxiliary amplifier supply voltage, $V_{\mathrm{GG},2}$ (see Fig. 1).

As reported in [9], for values higher than $p = 4$ the power efficiency starts dropping significantly, while there is a sweet spot for linearity, in terms of NMSE and ACPR, around the value of $p = 5$. With these results we can make a fine adjustment of this parameter setting the value of p between 3 and 5.

To analyze the effect of the auxiliary PA gate voltage, we carried out a sweep of $V_{\mathrm{GG},2}$ exciting the LMBA with an LTE-20 signal at 2 GHz, with an optimal phase shift of $\Psi_{rel} = 260°$ and $p = 3$. Fig. 10 shows how the NMSE and ACPR values get better for $V_{\mathrm{GG},2}$ between -3.5 V and -4 V, while slightly higher power efficiency (the maximum variation of power efficiency is only 0.5 percentage points) is observed for $V_{\mathrm{GG},2}$ between -3.9 V and -4.9 V.

IV. Digital Predistortion Linearization

Once the LMBA is properly tuned, the most suitable (in terms of linearization performance and computational complexity) linearization method is selected, as depicted in the flow chart of Fig. 2. In the following subsections we will describe both the polynomial-based DPD and the ANN-based DPD, providing specific details on the adaptation required to ensure reconfigurability to cope with dynamic environments.

A. Polynomial-Based Adaptive DPD

A common approach in literature for DPD is the use of behavioral models in the form of simplified versions of the full Volterra series. The generalized memory polynomial (GMP) is

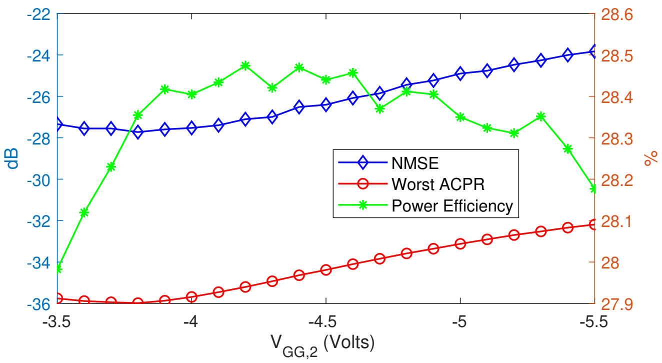

Fig. 10. LMBA linearity and power efficiency for different values of $V_{\mathrm{GG},2}$, considering an LTE-20 signal at 2 GHz.

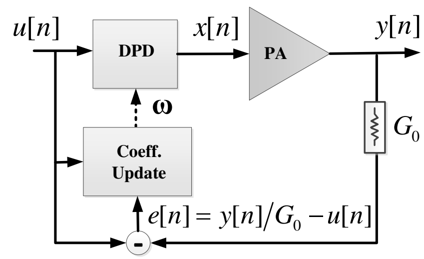

Fig. 11. Adaptive DPD architecture following a direct learning approach.

a popular candidate since it introduces bi-dimensional kernels (considering cross-term products between the complex signal and the lagging and leading envelope terms) which increase the capability to compensate for the PA memory effects. Following the notation of the block diagram in Fig. 11, the input-output relationship at the DPD block is defined as

$$x[n] = u[n] - d[n] \tag{4}$$

where $x[n]$ is the signal at the output of the DPD block, $u[n]$ is the input signal and $d[n]$ is an error signal that can be described following a generic GMP structure as

$$\begin{aligned} d(n) = & \sum_{l=0}^{L_a-1} u(n-l)\varphi_l^a(|u(n-l)|) \\ & + \sum_{l=0}^{L_b-1}\sum_{m=1}^{M_b} u(n-l)\varphi_{l,m}^b(|u(n-l-m)|) \\ & + \sum_{l=0}^{L_c-1}\sum_{m=1}^{M_c} u(n-l)\varphi_{l,m}^c(|u(n-l+m)|) \end{aligned} \tag{5}$$

where $\varphi(\cdot)$ are generic non-linear functions that depend on envelope terms. These nonlinear functions can be described by polynomials as in the case of the original GMP [19], or by B-splines as presented in [9]. In any case, the GMP is a parametric model that can be expressed as the linear combination of non-linear basis functions weighted by some parameters. In general, (4) can be rewritten in a matrix notation as,

$$\boldsymbol{x} = \boldsymbol{u} - \boldsymbol{U}\boldsymbol{w} \tag{6}$$

where $\boldsymbol{U}$ is the data matrix containing the DPD basis functions and $\boldsymbol{w}$ is the vector of parameters. By following a direct learning approach (see Fig. 11) the vector of parameters can be estimated iteratively as follows

$$\boldsymbol{w}^{j+1} = \boldsymbol{w}^j + \mu^j \left(\boldsymbol{U}^{\mathbf{H}}\boldsymbol{U}\right)^{-1}\boldsymbol{U}^{\mathbf{H}}\boldsymbol{e} \tag{7}$$

where μ^j is the learning ratio at iteration j and $\boldsymbol{e}$ is the DPD error vector defined as

$$\boldsymbol{e} = \frac{\boldsymbol{y}}{G_0} - \boldsymbol{u} \tag{8}$$

where G_0 determines the desired linear gain of the PA, and where $\boldsymbol{y}$ and $\boldsymbol{u}$ are the PA output and transmitted input data vectors, respectively.

B. Adaptive DPD Based on Artificial Neural Networks

The most commonly used ANN architecture for DPD linearization is the feedforward time-delayed neural network (FTDNN). In order handle complex data, real-valued (RV) FTDNN are used taking as inputs the in-phase (I) and quadrature (Q) components of the complex signal. Moreover, additional terms, such as envelope or phase terms, are included as inputs to the RV-FTDNN [16], [18], [20], to improve its linearization performance.

In order to select the different hyper-parameters of our ANN (such as the architecture of the network, the input variables, the number of hidden layers and the number of neurons per layer), we ran some preliminary tests to model the LMBA nonlinear behavior when excited with a challenging signal composed by 4 non-contiguous LTE-20 channels over a total bandwidth of 200 MHz. As a result, Fig. 12 shows the proposed RV-FTDNN network, composed of 4 hidden layers (i.e., $N_{HL} = 4$) and a distribution of 20, 20, 10 and 10 neurons per hidden layer, respectively. The input values correspond to the I and Q components of the signal (i.e, $u_I[n]$ and $u_Q[n]$ in Fig. 12), including time-delayed components up to a certain memory depth (e.g., 7 delay taps) and envelope dependent terms (i.e. $|u[n]|^p$ with $p = 1, \cdots, 4$) including also their time-delayed values. A total of $N_0 = 48$ inputs to the ANN were considered. After running several tests evaluating the performance obtained with different activation functions in the hidden layers of the ANN, the sigmoid tangent function was selected. It is mathematically equivalent to the hyperbolic tangent function but its Matlab implementation runs faster. Finally, a linear function was selected in the output layer.

Taking into account the RV-FTDNN depicted in Fig. 12 and considering an input layer with N_0 inputs, the input-output relationship for both I and Q components is defined in (9) and (10), respectively:

$$\begin{aligned} x_I[n] = & \sum_{s=1}^{N_4}\omega_{1,s}^5\ f^4\Bigg(\sum_{k=1}^{N_3}\omega_{s,k}^4\ f^3\Big(\sum_{j=1}^{N_2}\omega_{k,j}^3\ f^2\big(\sum_{l=1}^{N_1}\omega_{j,l}^2 \\ & f^1\big(\sum_{i=1}^{N_0}\omega_{l,i}^1\ \varphi_i[n]+\sigma_l^1\big)+\sigma_j^2\big)+\sigma_k^3\Big)+\sigma_s^4\Bigg)+\sigma_1^5 \end{aligned} \tag{9}$$

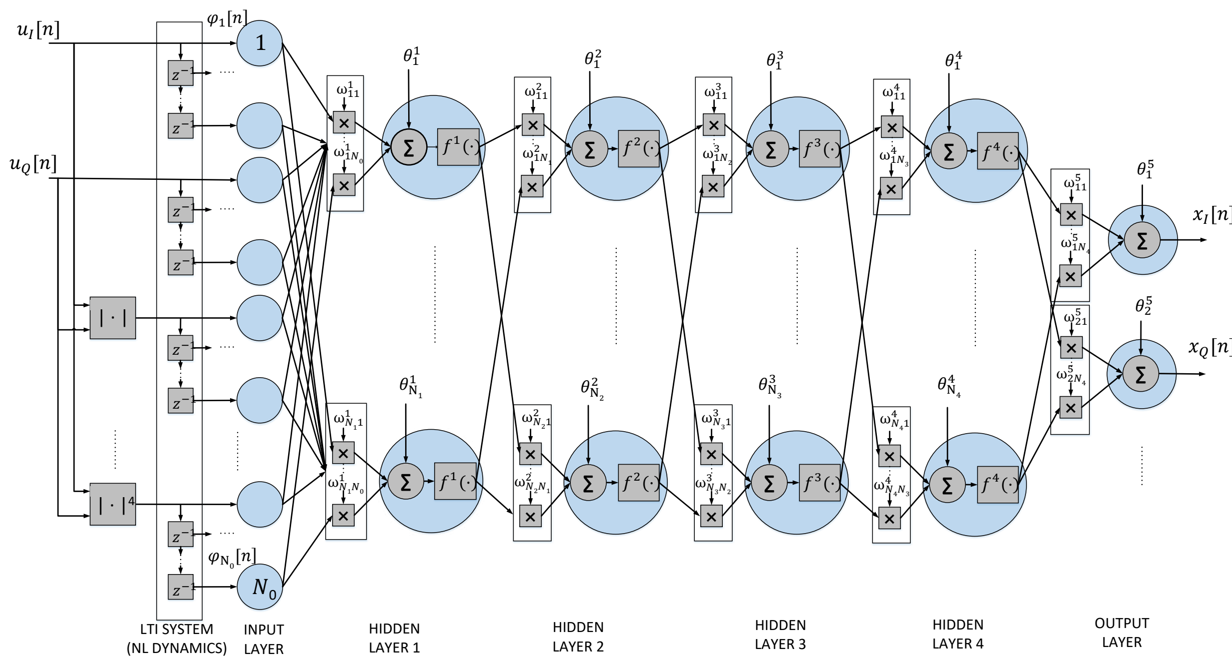

Fig. 12. RV-FTDNN network composed of 4 hidden layers and a distribution of $[N_1, N_2, N_3, N_4] = [20, 20, 10, 10]$ neurons per hidden layer.

$$x_Q[n] = \sum_{s=1}^{N_4} \omega_{2,s}^5 \; f^4\Bigg(\sum_{k=1}^{N_3} \omega_{s,k}^4 \; f^3\Big(\sum_{j=1}^{N_2} \omega_{k,j}^3 \; f^2\big(\sum_{l=1}^{N_1} \omega_{j,l}^2 \; f^1\big(\sum_{i=1}^{N_0} \omega_{l,i}^1 \; \varphi_i[n] + \sigma_l^1\big) + \sigma_j^2\big) + \sigma_k^3\Big) + \sigma_s^4\Bigg) + \sigma_2^5 \quad (10)$$

where $\varphi_i[n]$ with $(i = 1, \cdots, N_0)$ are the inputs to the ANN (e.g., $\varphi_1[n] = u_I[n], \varphi_2[n] = u_I[n-1]$, etc.), $\omega_{a,b}^m$ (with $m = 1, \cdots, N_{HL}+1$) are synaptic weights of the network, the values of σ_a^m are the bias, $f^r(\cdot)$ (with $r = 1, \cdots, N_{HL}$) are the activation functions and N_r are the number of neurons per hidden layer. As explained before, in our particular ANN for DPD purposes $N_{HL} = 4$ and $[N_1, N_2, N_3, N_4] = [20, 20, 10, 10]$. The number of coefficients of the proposed RV-FTDNN results from the sum of the number of weights and the number of biases, and thus $O = (N_0\, N_1 + N_1\, N_2 + N_2\, N_3 + N_3\, N_4 + 2\, N_4) + (N_1 + N_2 + N_3 + N_4 + 2)$.

ANN-based DPD can be applied adaptively or non-adaptively (i.e., in open-loop). If a non-adaptive scheme is chosen, the ANN coefficients are configured through prior training and remain fixed over time. However, if an adaptive implementation is considered, the coefficients of the ANN are updated by retraining the network over time. This implementation allows us to adjust the ANN DPD to time-varying LMBA behavior or to a dynamic environment where the transmitted signal characteristics change over time. For example, in systems where a general-purpose DPD has to cope with different signal bandwidths at different center frequencies or operating the PA with different output back-off levels, some reconfigurability of the DPD parameters is required. Therefore, although we start from an initial condition of the DPD parameters obtained in an off-line training, if we want the best DPD linearization performance for specific operating conditions (i.e., for a given signal input power, bandwidth, center frequency, etc.), coefficients adaptation is required.

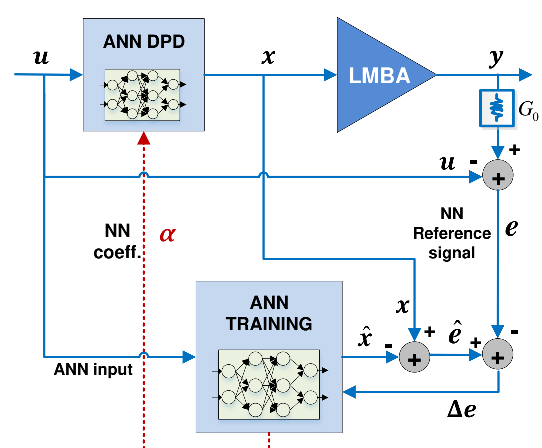

Fig. 13. Adaptive ANN-based DPD following a direct learning approach.

The block diagram in Fig. 13 shows the proposed adaptive ANN DPD implementation following a direct learning approach. The Levenberg-Marquardt (LM) backpropagation algorithm is used to calculate the RV-FTDNN coefficients by minimizing the mean square error (MSE) cost function C in (11) for each training data batch of length K samples. This forward-backward process is repeated until the desired modeling performance is met or the ANN fails in the validation procedure [21].

$$C = \frac{1}{2K} \sum_{n=1}^{K} \big(\hat{e}_I[n] - e_I[n]\big)^2 + \big(\hat{e}_Q[n] - e_Q[n]\big)^2 \qquad (11)$$
$$= \frac{1}{2K} \sum_{n=1}^{K} \left|\Delta e[n]\right|^2$$

where K is the data batch length and $\boldsymbol{\Delta e}$ is the data batch error vector (see Fig. 13) of K samples defined as,

$$\boldsymbol{\Delta e} = \hat{\boldsymbol{e}} - \boldsymbol{e} \tag{12}$$

with $\boldsymbol{e}$ being the residual linearization error vector defined in (8) and $\hat{\boldsymbol{e}}$ being the estimated residual linearization error defined as follows

$$\hat{\boldsymbol{e}} = \boldsymbol{x} - \hat{\boldsymbol{x}} \tag{13}$$

where $x[n] = x_I[n] + jx_Q[n]$ is the predistorted output signal and $\hat{x}[n] = \hat{x}_I[n] + j\hat{x}_Q[n]$ is the output signal (I/Q pairs) produced at the output layer of the training ANN, as depicted in Fig. 13. The cost function C is minimized according to the LM algorithm and with respect to the vector of coefficients $\boldsymbol{\alpha} = \left[w_{11}^1 \cdots w_{\mathrm{N_1 N_0}}^1 \theta_1^1 \cdots \theta_{\mathrm{N_1}}^1 \cdots w_{11}^5 \cdots w_{\mathrm{2N_4}}^5 \theta_1^5 \theta_2^5\right]^T$ containing the weights and biases of the RV-FTDNN. When going backwards, $\boldsymbol{\alpha}$ is updated at every epoch j as

$$\boldsymbol{\alpha}^{j+1} = \boldsymbol{\alpha}^j - \left(\boldsymbol{J}^T\boldsymbol{J} + \lambda\boldsymbol{I}\right)^{-1}\boldsymbol{J}^T\Delta\boldsymbol{e} \tag{14}$$

where $\boldsymbol{I}$ is the identity matrix, λ is the damping factor and $\boldsymbol{J}$ is the Jacobian matrix being calculated over the error vector $\boldsymbol{\Delta e}$ with respect to $\boldsymbol{\alpha}$ as

$$\boldsymbol{J} = \begin{pmatrix} \frac{\partial \Delta e[1]}{\partial w_{11}^1} & \frac{\partial \Delta e[1]}{\partial w_{12}^1} \cdots & \frac{\partial \Delta e[1]}{\partial \theta_1^5} & \frac{\partial \Delta e[1]}{\partial \theta_2^5} \\ \frac{\partial \Delta e[2]}{\partial w_{11}^1} & \frac{\partial \Delta e[2]}{\partial w_{12}^1} \cdots & \frac{\partial \Delta e[2]}{\partial \theta_1^5} & \frac{\partial \Delta e[2]}{\partial \theta_2^5} \\ & \vdots & & \\ \frac{\partial \Delta e[K]}{\partial w_{11}^1} & \frac{\partial \Delta e[K]}{\partial w_{12}^1} \cdots & \frac{\partial \Delta e[K]}{\partial \theta_1^5} & \frac{\partial \Delta e[K]}{\partial \theta_2^5} \end{pmatrix} \tag{15}$$

Fig. 14 presents a comparison of the linearization performance (in terms of ACPR) versus number of averages of the measured PA output signal, when considering adaptation and open-loop ANN DPD. The ACPR results shown with the adaptive DPD were obtained after 3 update iterations (independently of the number of averages considered) from the initial configuration of parameters. This initial parameter estimation was carried out in a preliminary off-line training and corresponds to the parameter configuration that is permanently used in the open-loop (non-adaptive) DPD. As it will be further described in section V, the test signal used consisted of 4 non-contiguous LTE-20 channels over a total bandwidth of 200 MHz. It is well-known that, considering the test bench described in section V, by averaging several captures of the PA output signal we can reduce the noise floor and thus enhance the DPD linearization capabilities. Consequently, a straightforward conclusion derived from the results depicted in Fig. 14 is that adaptive DPD, with proper averaging, can outperform the spectral regrowth compensation obtained by the open-loop ANN DPD by more than 4 dB.

One of the main problems of the adaptive ANN DPD, besides the computational complexity, is the required training time for each update. In order to reduce the retraining time between adaptations we have followed two approaches: limiting the number of ANN training epochs and reducing the number of training samples. Several techniques have been proposed

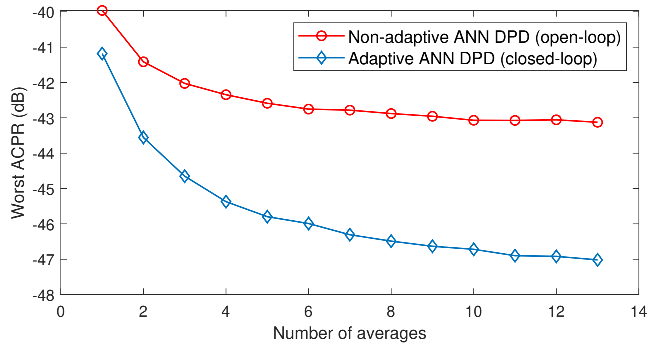

Fig. 14. ACPR values for an adaptive and non-adaptive implementation of the ANN DPD for different number of averages.

in literature to select the most relevant training data allowing a reliable estimation without significant loss of performance [18], [22]. In this paper we have used the mesh selecting method proposed in [22].

V. Experimental Test Bench and Results

A. Experimental Test Bench

The dual-input PA system was experimentally evaluated using a Matlab-controlled digital linearization test bench, as shown in Fig. 15, interfacing waveform generation and acquisition instruments. In order to compensate for the out-of-band distortion, a 614.4 MSa/s DPD signal was digitally up-converted to the 2 GHz RF frequency, and digital to analog converted (through the AWG M8190A from Keysight, with a clock rate of 7.9872 GHz and 14 bits) to feed the dual-input PA. The PA output signal was attenuated, RF sampled with the digital storage oscilloscope (DSO) Keysight 90404A at 20 GSa/s with 8-bit resolution (applying averages to reduce the noise floor), digital down-converted and resampled for time-alignment and DPD processing. A Keysight N9020A MXA signal analyzer was used to characterize the spectrum at the output of the PA.

The data set used for off-line training the ANN consisted of 307200 complex-valued data samples. The estimated parameters of the ANN were later validated and eventually adapted (in a different time-scale than real-time) in closed-loop DPD using different batches of 307200 complex-valued data samples at each iteration. In the case of the GMP-based DPD, no off-line training was applied a priori. Instead, the coefficients were directly adapted from scratch in the DPD observation loop considering also different batches of 307200 complex-valued data samples at each iteration.

B. GMP versus ANN DPD for Different Signal Bandwidths at 2 GHz RF Center Frequency

In a first approach, we wanted to evaluate when (or if) it is worth using ANNs instead of simplified Volterra series behavioral models, such as the GMP. Even though ANNs can outperform the linearization capabilities of polynomial-based behavioral models, the price to pay is an increase of computational complexity, for example, stated in terms of number of parameters. Therefore, with this objective in mind,

TABLE I
COMPARISON OF ANN-BASED AND GMP-BASED DPD FOR DIFFERENT TEST SIGNALS AT 2 GHZ RF CENTER FREQUENCY.

DPD type	Signal type	Worst ACPR	NMSE	EVM	Num. Coff.
No DPD		-35.0 dB	-26.4 dB	2.4 %	—
GMP	64-QAM LTE-20, BW=20 MHz	-51.0 dB	-39.3 dB	0.7 %	248
ANN (mem. depth =7)		-52.9 dB	-40.4 dB	0.6 %	1742
No DPD		-32.1 dB	-24.1 dB	2.7 %	—
GMP	NC 64-QAM 2×LTE-20, BW=60 MHz	-51.0 dB	-39.6 dB	0.6 %	248
ANN (mem. depth =7)		-49.9 dB	-39.2 dB	0.6 %	1742
No DPD		-28.4 dB	-19.8 dB	4.7 %	—
GMP	NC 64-QAM 4×LTE-20, BW=200 MHz	-35.4 dB	-28.0 dB	2.1 %	248
ANN (mem. depth =7)		-44.0 dB	-35.9 dB	0.7 %	1742
ANN (mem. depth =9)		-46.2 dB	-36.3 dB	0.9 %	1982

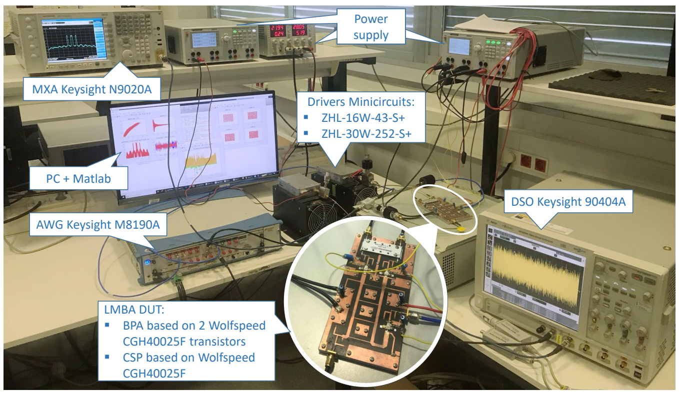

Fig. 15. Laboratory test bench including the LMBA used as DUT.

the LMBA was excited with different test signals in order to evaluate linearization performance of both ANN-based and GMP-based DPD linearizers. The test signals' characteristics as well as the LMBA delivered output power and power efficiency achieved with these signals are described in the following:

1) A 64-QAM LTE-20 signal of 20 MHz total bandwidth, centered at 2 GHz and with 10.2 dB of PAPR. With this test signal the LMBA was operated to deliver around 35.5 dBm mean output power with a power efficiency around 28%.
2) 2 non-contiguous 64-QAM LTE-20 (NC 2×LTE-20) signal of 60 MHz total bandwidth, centered at 2 GHz and with 10.4 dB of PAPR. With this test signal the LMBA was operated to deliver around 35.5 dBm mean output power with a power efficiency around 28%.
3) 4 non-contiguous 64-QAM LTE-20 (NC 4×LTE-20) signal of 200 MHz total bandwidth centered at 2 GHz and with 10.6 dB of PAPR. With this test signal the LMBA was operated to deliver around 33.3 dBm mean output power with a power efficiency around 21.4%.

The initial configuration of parameters for both GMP and the ANN DPD behavioral models was rich enough to be able to cope with the worst-case scenario, i.e., the linearization of the NC 4×LTE-20 signal. Therefore, as listed in Table I, the same amount of coefficients were used to address the linearization of all three type of signals. Having an initial condition for the GMP parameters is not critical, since the parameters identification is relatively fast. However, in the case of ANNs, the training time can be significantly long. Consequently, it is of crucial importance to speed up the adaptation process to have an accurate initial condition of the ANN parameters. For that reason, targeting an agile, versatile operation, the ANN was initially trained considering the NC 4×LTE-20 signal of 200 MHz total bandwidth. Once the ANN is trained, it can be used as a DPD for different signals with different bandwidth.

The training time for ANNs depends on several factors such as: the hyper-parameters of the ANN (number of hidden layers, neurons, etc.), the available hardware to carry out the computation (e.g., hardware accelerators such as GPUs or FPGAs), the software/library used (e.g., Matlab, Pytorch), the type of solver used, the batch size or the number of epochs. For the off-line training of the ANN parameters (i.e., the initial condition), we used the LM algorithm provided by Matlab without hardware accelerators, considering a batch size of 307200 samples and without imposing limitations on the number of epochs. Consequently, the training time was around 6 hours. However, once the initial condition for the ANN coefficients was estimated, in order to reduce the retraining time between adaptations, we followed two approaches: limiting the number of ANN training epochs and reducing the number of training samples using the mesh selecting method proposed in [22]. Then, the retraining time was reduced to a few minutes. In particular, between 2 and 5 minutes depending on the number of selected data samples to carry out the adaptation (there is a trade-off between computational complexity and modeling accuracy).

Table I shows the linearization performance (in terms of ACPR, NMSE and EVM), of both the ANN-based and GMP-based DPD linearizers when considering the previously described test signals. The nonlinear functions in the general GMP behavioral model in (5) are particularized with polynomials. Therefore, the metaparameters configuration of the GMP DPD used in this paper is: nonlinear order of $Pa = 7$, $Pb = 5$, $Pc = 5$ and memory depth of $Ma = 9$, $Mb = 7$, $Mc = 7$, $Qb = 2$, $Qc = 2$; corresponding to a total of 248 coefficients. This configuration was selected to have two general-purpose DPD linearizers (i.e., the GMP-based and the ANN-based) with the same memory depth. Even if the GMP and ANN are not specifically dimensioned (i.e., use the minimum required number of coefficients to meet the linearity specs) to linearize the 20 MHz or the 60 MHz total bandwidth signals, it is clear that GMP DPD can perfectly cope with the compensation of the nonlinear distortion and memory effects by meeting the targeted ACPR<-45 dB, with significantly less computational complexity than ANNs. Taking into account the aforementioned GMP configuration with 248 coefficients, the time for running the coefficients estimation (1 iteration) was less than 10 seconds considering Matlab's backslash operation.

However, when considering the NC 4×LTE-20 signal of 200 MHz total bandwidth, the GMP DPD is not capable to meet the required ACPR levels. By increasing the number of coefficients of the GMP model, not only there is no improvement in the spectral regrowth compensation, but it also leads to an ill-conditioned and unreliable estimation of the coefficients. In general, the bi-dimensional kernels of the GMP architecture represent a good trade-off between computational complexity and nonlinear dynamic modeling capabilities. But yet, the GMP is still a simplified version of the Volterra series covering a much more reduced area in the kernel space than the original Volterra series. Therefore, when dealing with wideband signals (e.g., hundreds of MHz), the inherent limitation of the GMP architecture for covering certain cross-memory products can prevent meeting the required ACPR levels, regardless of whether regularization or feature selection techniques are applied. Consequently, in this particular demanding situation, the use of ANNs is justified. Note that the ANN with a memory depth of 7 taps still cannot meet the targeted ACPR level, and thus, the memory depth has to be increased up to 9 taps to go beyond the minimum -45 dB of ACPR. Fig. 17 and Fig. 16 show the AM-AM characteristics and output power spectra before and after DPD linearization using GMP and ANN DPD, respectively. It is evident that the ANN DPD clearly outperforms the GMP DPD for wide-band signals where memory effects are critical, and the ANN can take advantage of the internal interactions that occur in its hidden layers.

C. Linear and Power Efficient LMBA Amplification from 1.8 to 2.4 GHz Considering Different Transmitted Signals

In order to guarantee linear and power efficient amplification for dual-input PAs such as the DUT used in this work, we have proposed the methodology described in the flow diagram of Fig. 2. Therefore, assuming a dynamic environment where the transmitted signal to be amplified by the LMBA can present different bandwidths and operate at different center frequencies in the range of 1.8 to 2.4 GHz, we will proceed as follows (see Fig. 2):

- First, assuming that the delay value has been previously determined and fixed, the optimum phase shift between the BPA and CSP signals is calculated. For a given input signal with a certain bandwidth and at a specific center frequency, we will use the extracted phase-shift model to determine the best phase-shift between the LMBA input signals.
- Then, it is necessary to determine the values of p and $V_{\mathrm{GG},2}$ for trading-off linearity and power efficiency as described in subsection III-C. For example, for the experimental results presented in Table II, we have considered $p = 3.5$ and $V_{\mathrm{GG},2} = -4.2$ V.

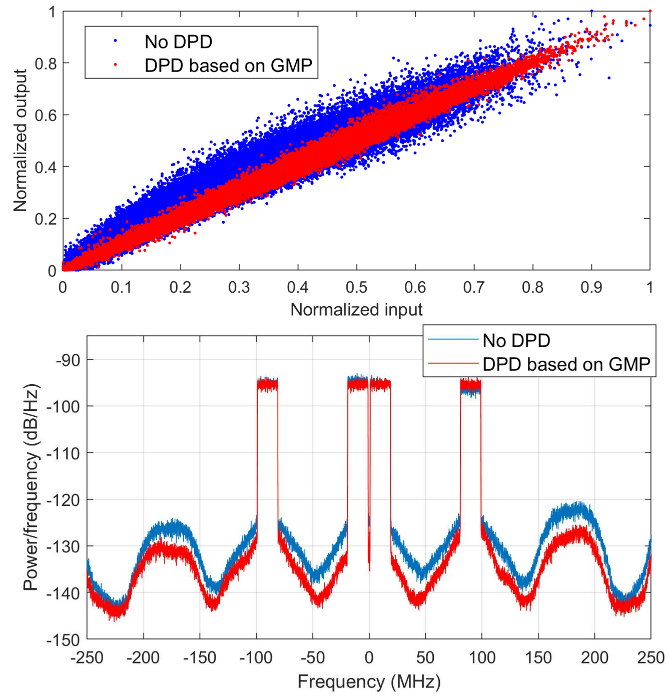

Fig. 16. AM-AM characteristics (top) and output power spectra (bottom) before and after GMP-based DPD linearization, considering a NC 4×LTE-20 signal at 2 GHz RF center frequency.

- A crest factor reduction (CFR) technique is used to limit the PAPR of the signal. A well-known strategy commonly used in literature is to reduce the PAPR of the signal to be able to operate the PA with less back-off and thus more power efficiently. In this work, we have considered the peak cancellation CFR technique as described in [23].
- Then, according to the transmitted signal characteristics we decide the DPD strategy. For example, in our particular test case, for signals exceeding 60 MHz total bandwidth, the linearization is carried out by means of an ANN-based DPD. Otherwise, for signals with up to 60 MHz total bandwidth, the less computationally intensive GMP DPD is considered. It is worth mentioning that the ANN-based DPD would be enough to linearize any type of the test signals considered, however, at the price of introducing additional computational complexity (with respect to GMP) when it is not strictly required.
- Finally, from a given initial condition (obtained in an off-line training) the adaptive DPD periodically updates its coefficients to meet the required linearity specifications. If the bandwidth or the center frequency of the transmitted signal changes (for example, because other LTE-20 channels are aggregated), then the LMBA linearization system has to be reconfigured again, as schematically described in Fig. 2.

In order to validate the proposed methodology, Table II shows how the linearity specifications are met under different transmitted signal configurations in terms of bandwidth (BW) and center frequency (F_c) of operation. As an example, Fig. 19 and Fig. 20 show the spectra of the NC 2×LTE-20 signal of 60 MHz total bandwidth and the LTE-20 signal,

TABLE II

LINEARITY AND POWER EFFICIENCY RESULTS OF THE LMBA OPERATED WITH TRANSMITTED SIGNALS WITH DIFFERENT BANDWIDTH CONFIGURATIONS IN THE RF RANGE OF 1.8 TO 2.4 GHZ.

Signal configuration	DPD	Nº Coeff.	PAPR	Worst ACPR	NMSE	Pout	Efficiency	EVM
Fc = 2.2 GHz, BW = 200 MHz	ANN	1982	9 dB (with CFR)	-46.1 dB	-32.9 dB	33.0 dBm	16.7 %	1.2 %
Fc = 1.9 GHz, BW = 20 MHz	GMP	248	9 dB (with CFR)	-48.0 dB	-37.7 dB	38.3 dBm	38.5 %	0.8 %
Fc = 2.1 GHz, BW = 60 MHz	GMP	248	10.2 dB	-51.2 dB	-38.3 dB	37.1 dBm	31.1 %	0.7 %
Fc = 1.8 GHz, BW = 200 MHz	ANN	1982	8 dB (with CFR)	-46.1 dB	-27.2 dB	32.4 dBm	18.6 %	2.7 %

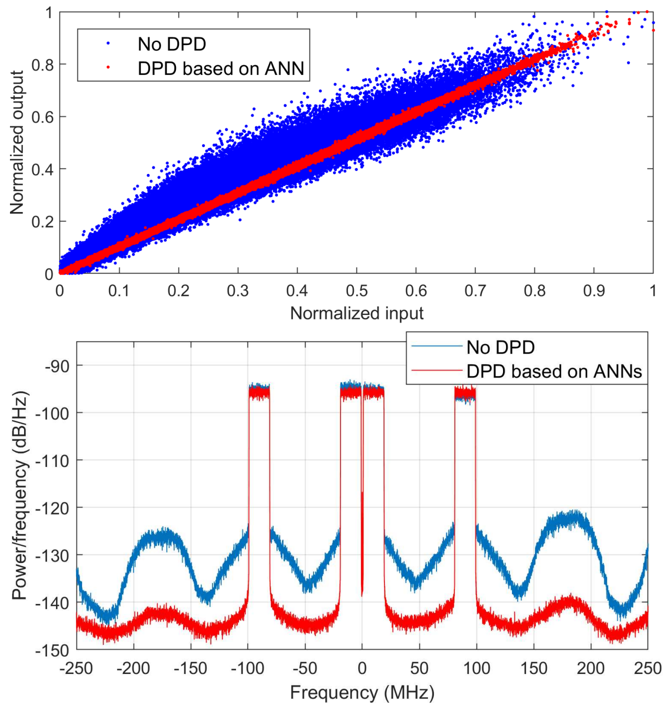

Fig. 17. AM-AM characteristics (top) and output power spectra (bottom) before and after ANN-based DPD linearization, considering a NC 4×LTE-20 signal at 2 GHz RF center frequency.

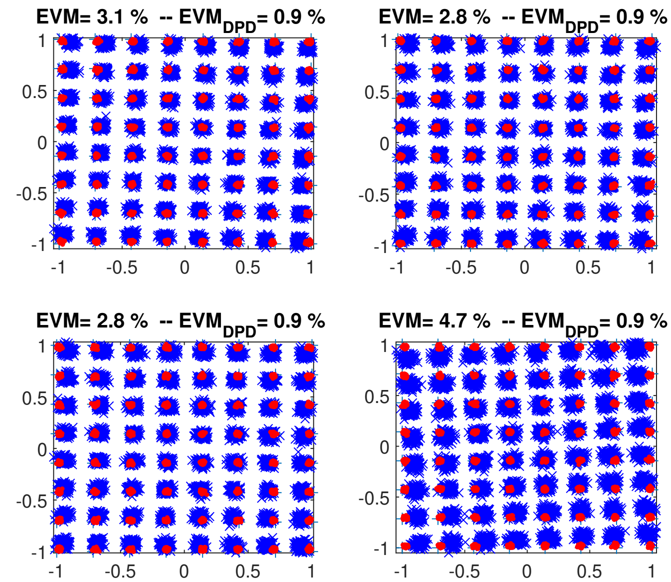

Fig. 18. 64-QAM constellations of the NC 4×LTE-20 signal at 2 GHz RF center frequency8 before and after ANN-based DPD linearization.

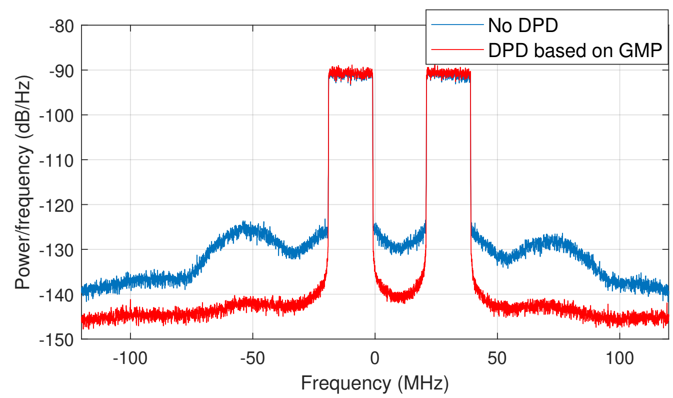

Fig. 19. Linearized and unlinearized output power spectra with GMP-based DPD considering a NC 2×LTE-20 signal at 2.1 GHz RF center frequency.

respectively, before and after GMP-based DPD linearization. When limiting the maximum PAPR of the signal (by means of the peak cancellation CFR technique) it is possible to push the input signal harder into compression to slightly improve the overall drain efficiency, but at the price of introducing in-band distortion (as reflected in the NMSE and EVM figures in Table II). Notice that the LMBA linear mean output power and power efficiency change not only with the bandwidth of the transmitted signal, but also with the center frequency of operation, as depicted in Fig. 7.

VI. CONCLUSION

In this paper, we propose a methodology to ensure linear amplification of a dual-input PA that can operate in a dynamic environment over a frequency range from 1.8 to 2.4 GHz. In a first step, some parameters defining the LMBA operation mode are properly tuned, taking into account the center frequency of operation to ensure linearizability with maximum power efficiency. In a second step, CFR and DPD linearization techniques are used to meet the required linearity specifications. An ANN-based DPD is previously trained off-line to be able to cope with different signal bandwidths. By including adaptation, the ANN is able to meet the linearity specifications for any signal bandwidth configuration. However, given the computational complexity introduced by the ANN, for less challenging scenarios (e.g., in our particular case, we considered signals with $BW \leq 60$ MHz) a less computational complex GMP-based DPD is selected.

In the path towards allowing total reconfigurability of the amplification system, machine learning techniques will be included in future works to allow fine tuning of the LMBA free

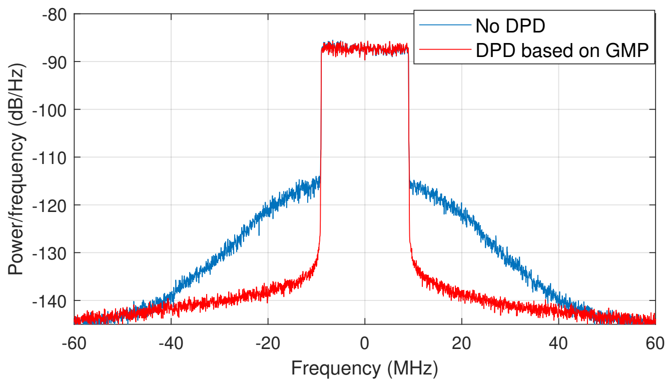

Fig. 20. Linearized and unlinearized output power spectra with GMP-based DPD considering an LTE-20 signal at 1.9 GHz RF center frequency.

parameters oriented at maximizing power efficiency for each frequency of operation and transmitted signal characteristics.

References

[1] Z. Wang, "Demystifying envelope tracking: Use for high-efficiency power amplifiers for 4G and beyond," *IEEE Microw. Mag.*, vol. 16, no. 3, pp. 106–129, Apr. 2015.

[2] V. Camarchia, M. Pirola, R. Quaglia, S. Jee, Y. Cho, and B. Kim, "The doherty power amplifier: Review of recent solutions and trends," *IEEE Trans. Microw. Theory Techn.*, vol. 63, no. 2, pp. 559–571, Feb. 2015.

[3] R. Pengelly, C. Fager, and M. Ozen, "Doherty's legacy: A history of the Doherty power amplifier from 1936 to the present day," *IEEE Microw. Mag.*, vol. 17, no. 2, pp. 41–58, Feb. 2016.

[4] D. J. Shepphard, J. Powell, and S. C. Cripps, "An efficient broadband reconfigurable power amplifier using active load modulation," *IEEE Microw. Wireless Compon. Lett.*, vol. 26, no. 6, pp. 443–445, June 2016.

[5] R. Quaglia and S. Cripps, "A Load Modulated Balanced Amplifier for Telecom Applications," *IEEE Trans. Microw. Theory Techn.*, vol. 66, no. 3, pp. 1328–1338, Mar. 2018.

[6] Z. Popovic and J. A. Garcia, "Microwave Class-E Power Amplifiers: A Brief Review of Essential Concepts in High-Frequency Class-E PAs and Related Circuits," *IEEE Microw. Mag.*, vol. 19, no. 5, pp. 54–66, Jul. 2018.

[7] M. Litchfield and T. Cappello, "The various angles of outphasing PAs: Competitiveness of outphasing in efficient linear PA applications," *IEEE Microw. Mag.*, vol. 20, no. 4, pp. 135–145, Apr. 2019.

[8] R. Ma, M. Benosman, K. A. Manjunatha, Y. Komatsuzaki, S. Shinjo, K. H. Teo, and P. V. Orlik, "Machine-learning based digital doherty power amplifier," in *Proc. IEEE Int. Symp. on Radio-Freq. Integration Technol. (RFIT)*, Melbourne, VIC, Australia, Aug. 2018, pp. 1–3.

[9] E. Guillena, W. Li, P. L. Gilabert, and G. Montoro, "Prediction of the optimal phase shift between control signals in dual-input power amplifiers," in *Proc. Int. Workshop on Integr. Nonlinear Microw. and Millimetre-Wave Circuits (INMMiC)*, Cardiff, UK, Jul. 2020, pp. 1–3.

[10] K. Vivien, P. E. de Falco, G. Baudoin, O. Venard, P. P. C. Felix, and T. Barton, "Load modulated balanced amplifier designed for AM-PM linearity," in *Proc. 50^{th} Eur. Microw. Conf. (EuMC)*, Utrecht, Netherlands, Jan. 2021, pp. 304–307.

[11] R. Quaglia, J. Powell, D. Shepphard, P. Tasker, and S. Cripps, "Analysis and characterization of a load modulated balanced amplifier for base-station applications," in *Proc. 11^{th} German Microw. Conf. (GeMiC)*, Freiburg, Germany, Mar. 2018, pp. 1–4.

[12] D. Collins, R. Quaglia, J. Powell, and S. Cripps, "Experimental characterization of a load modulated balanced amplifier with simplified input power splitter," in *Proc. Asia-Pacific Microw. Conf. (APMC)*, Kyoto, Japan, Nov. 2018, pp. 461–463.

[13] T. Cappello, P. H. Pednekar, C. Florian, Z. Popovic, and T. W. Barton, "Supply modulation of a broadband load modulated balanced amplifier," in *IEEE MTT-S Int. Microw. Symp. Dig.*, Philadelphia, PA, USA, Jun. 2018, pp. 304–307.

[14] T. Cappello, P. Pednekar, C. Florian, S. Cripps, Z. Popovic, and T. W. Barton, "Supply- and load-modulated balanced amplifier for efficient broadband 5G base stations," *IEEE Trans. on Microw. Theory and Techn.*, vol. 67, no. 7, pp. 3122–3133, Jul. 2019.

[15] J. Pang, Y. Li, M. Li, Y. Zhang, X. Y. Zhou, Z. Dai, and A. Zhu, "Analysis and design of highly efficient wideband RF-input sequential load modulated balanced power amplifier," *IEEE Trans. on Microw. Theory and Techn.*, vol. 68, no. 5, pp. 1741–1753, May 2020.

[16] D. Wang, M. Aziz, M. Helaoui, and F. M. Ghannouchi, "Augmented real-valued time-delay neural network for compensation of distortions and impairments in wireless transmitters," *IEEE Trans. on Neural Netw. and Learn. Syst.*, vol. 30, no. 1, pp. 242–254, Jan. 2019.

[17] M. Rawat, K. Rawat, and F. Ghannouchi, "Adaptive digital predistortion of wireless power amplifiers/transmitters using dynamic real-valued focused time-delay line neural networks," *IEEE Trans. Microw. Theory Techn.*, vol. 58, no. 1, pp. 95–104, Jan. 2010.

[18] D. López-Bueno, P. L. Gilabert, and G. Montoro, "Dataset reduction for neural network based digital predistorters under strong nonlinearities," in *Proc. IEEE Topical Conf. on RF/Microw. Power Amplifiers for Radio and Wireless Appl. (PAWR)*, San Diego, CA, Jan. 2021, pp. 1–4.

[19] D. R. Morgan, Z. Ma et al., "A Generalized Memory Polynomial Model for Digital Predistortion of RF Power Amplifiers," *IEEE Trans. Signal Process.*, vol. 54, no. 10, pp. 3852–3860, Oct. 2006.

[20] P. Jueschke and G. Fischer, "Machine learning using neural networks in digital signal processing for RF transceivers," in *Proc. IEEE AFRICON*, Cape Town, South Africa, Sep. 2017, pp. 384–390.

[21] S. S. Haykin, *Neural networks and learning machines*, 3rd ed. Upper Saddle River, NJ: Pearson Education, 2009.

[22] T. Wang and P. L. Gilabert, "Mesh-selecting for computational efficient PA behavioral modeling and DPD linearization," *IEEE Microw. Wireless Compon. Lett.*, vol. 31, pp. 37–40, Jan. 2021.

[23] D. López, P. L. Gilabert, G. Montoro, and N. Bartzoudis, "Peak cancellation and digital predistortion of high-order QAM wideband signals for next generation wireless backhaul equipment," in *Proc. Int. Workshop on Integr. Nonlinear Microw. and Millimetre-Wave Circuits (INMMiC)*, Leuven, Belgium, Apr. 2014, pp. 1–3.

Estefanía Guillena (Graduate Student Member, IEEE) received the double bachelor's degree in aerospace systems engineering and telecommunications systems engineering from the Universitat Politècnica de Catalunya in 2020. She joined the Components and Systems for Communications Research Group in 2019 to develop her bachelor's thesis in the field of power amplifier linearization. Estefanía was awarded with a Microwave Theory and Techniques Society (MTT-S) undergradute scholarship in April 2019. She is currently working for Dares Technology in the field of image processing as a Remote Sensing Engineer.

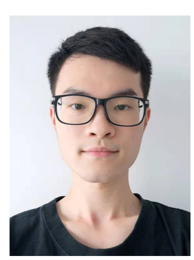

Wantao Li (Graduate Student Member, IEEE) was born in Canton, China, in 1995. He received the B.E. degree in electronic information science and technology from Beijing Union University, in 2017 and the M.S. degree in unmanned aircraft systems from Universitat Politècnica de Catalunya (UPC), in 2020. He joined the Components and Systems for Communications (CSC) Research Group in 2020 and he is currently pursuing his Ph.D. in the department of Signal Theory and Communications of the UPC. His research interests include signal processing for communication systems, power amplifier linearization and the efficient RTL implementations in FPGA.

Gabriel Montoro (Member, IEEE) received the M.Sc. degree in telecommunication engineering and the Ph.D. degree from the Universitat Politècnica de Catalunya (UPC), Barcelona, Spain, in 1990 and 1996, respectively. He joined the Department of Signal Theory and Communications (TSC) in 1991, where he is currently an Associate Professor. His first research works were done on the area of adaptive control, and now his main research interest is in the use of signal processing strategies for power efficiency improvement in communications systems.

Roberto Quaglia (Member, IEEE) was born in Casale Monferrato, Italy, in 1984. He graduated *cum laude* in electronic engineering from Politecnico di Torino in 2008. In 2012, he received the Ph.D. degree in electronic devices from the Politecnico di Torino, Turin, Italy. His research interests concern the design, modeling and predistortion of high efficiency MMIC power amplifiers, and he is currently a Lecturer at the School of Engineering of Cardiff University. He is a member of the IEEE MTT-TC 12. Dr. Quaglia was the recipient of a European Union Marie Skłodowska Curie fellow in 2015, and of the 2009 Young Graduated Research Fellowship presented by the GAAS Association.

Pere L. Gilabert (Senior Member, IEEE) received his M.Sc. degree in telecommunication engineering from the Universitat Politècnica de Catalunya (UPC) in 2002, and he developed his master's thesis at the University of Rome "La Sapienza" with an Erasmus exchange grant. He joined the department of Signal Theory and Communications in 2003 and received his Ph.D., awarded with the Extraordinary Doctoral Prize, from the UPC in 2008. He is an Associate Professor at the Castelldefels School of Telecommunications and Aerospace Engineering. His research activity is in the field of linearization techniques and digital signal processing solutions for highly efficient transmitter architectures.